Available online at www.sciencedirect.com
SCIENCE DIRECT®
PERGAMON
International Journal of Heat and Mass Transfer 46 (2003) 3909–3926
International Journal of HEAT and MASS TRANSFER
www.elsevier.com/locate/ijhmt

Computation of low Mach thermical flows with implicit upwind methods

Eric Schall [a,*], Cecile Viozat [b], Bruno Koobus [c], Alain Dervieux [d]

[a] IUT Génie Thermique et Energétique, 1, Avenue de l'Université, 64 000 Pau, France
[b] 47 av. Gal Dossin de St Georges, 1050 Bruxelles, Belgium
[c] Département de Mathématiques, Laboratoire ACSIOM (Analyse, Calcul Scientifique et Optimisation de Montpellier), FRE 2311 du CNRS, Université Montpellier II, Case Courrier 51, 34095 Montpellier Cedex 5, France
[d] INRIA, 2003 Route des Lucioles, F-06902 Sophia-Antipolis Cedex, France

Received 24 January 2002; received in revised form 27 January 2003

Abstract

In order to apply a Godunov method to steady and unsteady thermical flows, we first present a truncation error analysis which proves that the Turkel preconditioned Roe splitting is applicable to flows modelized by the classical low Mach number model, including thermics. The impact of the Turkel preconditioning on the first-order/second-order pseudo-Newton algorithm (referred in the literature as the defect-correction iteration) is also analysed. Implicit methods for steady flow resolution and for accurate unsteady time advancing are proposed and studied. Numerical illustrations involve the natural convection in a square box and a flow around a perforated wall inspired by helicopter engine applications.

Keywords: Low Mach flows; Thermical flows; Flux splitting; Implicit scheme; Time stepping methods

1. Introduction

Gas flows with regions where the Mach number is small introduce some difficulties in numerical simulations.

Several asymptotical models have been introduced in order to address the specific difficulties of the low Mach number; they are referred as the dilatable or low Mach number model [13], the Boussinesq model and the incompressible model.

Adapted numerical methods have been derived for these models: implicit pressure iteration, mesh staggering and mixed finite element ... but using these methods has some drawbacks:

- adapted methods lead to adapted software kernels or to much more complex software systems;
- asymptotic methods are less accurate at the limit of their application domain (when the Mach number is not so small) and not applicable to some mixed conditions (low Mach in some part of the geometry, larger Mach in another part).

It is therefore interesting to use a full compressible model, as far as it exhibits enough good features in term of robustness, cost efficiency and accuracy.

However, the application of a numerical method devoted to transonic flow computations to a low Mach flow may lead to several problems:

(i) generally, no adimensionalization is introduced for the low Mach number ("Euler number"), large numbers are then handled, and round off errors can become dominant;

* Corresponding author. Fax: +33-5-59-92-33-82.
E-mail addresses: eric.schall@univ-pau.fr (E. Schall), viozat@voila.fr (C. Viozat), koobus@darboux.math.univ-montp2.fr (B. Koobus), alain.dervieux@inria.fr (A. Dervieux).

0017-9310/03/$ - see front matter © 2003 Elsevier Ltd. All rights reserved.
doi:10.1016/S0017-9310(03)00178-9

Nomenclature

$Ec = \dfrac{u_*^2}{\varepsilon_*}$ Eckert number

$Fr = \dfrac{u_*^2}{g_* l_*}$ Froude number

$Pe = \dfrac{\rho_* u_* \varepsilon_* l_*}{k_* T_*}$ Péclet number

$St = \dfrac{l_*}{u_* t_*}$ Strouhal number

$Eu = \dfrac{p_*}{\rho_* u_*^2}$ Euler number

$Nu_{y=0} = \dfrac{k \dfrac{\partial T}{\partial x_{y=0}}}{k \dfrac{T_{\text{warm}} - T_{\text{cold}}}{l}}$ Nusselt number at $y = 0$

$Re = \dfrac{\rho_* u_* l_*}{\mu_*}$ Reynolds number

$\varepsilon_* = C_{v*} T_*$ internal energy

(ii) explicit methods can be used only with extremely small time steps and the systems to solve for steady solutions or long time unsteady ones are stiff;
(iii) with some numerical schemes, the approximation errors become very large for a given mesh.

Difficulty (i) is generally cured by adimensionalisation or the use of a decomposition between mean value and fluctuation.

Difficulty (ii) has been addressed by block-diagonal preconditioning. This preconditioning has been derived early by Turkel [16,17] who got inspired from the artificial compressibility method. Later, many authors (see for example [17,18]) have proposed smarter and smarter preconditioners for the fast pseudo-unsteady resolution of steady low Mach flows.

In the case of a Godunov-type scheme, it was observed that not only the convergence was accelerated, but also the solution was of good quality, in contrast to the non-preconditioned case. This gives also an answer to the third difficulty (iii).

We can also mention the work of Wesseling et al. [22] in which methods developped for the incompressible case are modified (leading to staggered schemes) for computing compressible flows with low Mach number regions.

Applications to quasi-incompressible flows were most frequently addressed, although applications with thermics were also presented [12,15].

The analysis of the original and preconditioned schemes have been also proposed for the convergence to incompressible. In particular, Guillard and Viozat [10] have put in evidence that non-preconditioned Godunov methods produced pressure fluctuation of a wrong order of magnitude with respect to the Mach number.

In this paper, we revisit the adaptation of a family of Godunov methods to low Mach flow calculations including thermics. More precisely, we consider a second-order MUSCL extension for Roe's upwind scheme, and the time advancing is implicit with a linearised preconditioner relying on first-order upwinding.

Several important questions are either not solved in the literature or deserve more accurate statements. They involve:

- the analysis of asymptotical accuracy for a large set of asymptotic flows including thermics,
- the convergence to steady-state of a pseudo-Newton iteration, assuming that the linear system is properly solved,
- the building of accurate implicit time advancing scheme.

1.1. Asymptotical accuracy

The basic mechanism of Godunov methods leads to add to each characteristic wave of an hyperbolic process a viscosity proportional to its velocity. But since the time is advanced with conservative variables, which are combinations of characteristic variables, this introduces some unfavourable cross influence between the stabilisation terms. As a result, for low Mach numbers, Godunov methods are too dissipative for the velocity, not enough for pressure, and in practice not applicable to Mach numbers less than one-tenth. Many authors have analysed the evolution of the truncation error when solutions are closer and closer to incompressible flows. The actual non-convergence of the discrete solution to the incompressible one has been established by Guillard and Viozat [10]. Conversely, a family of "preconditioned" flux splittings has been derived [18] and analysed as consistent approximations for incompressible flows. From our opinion, many authors have also intuited that *a larger family of low Mach number asymptotics including thermics* is affordable with the new schemes [15]. In this paper, we propose a reliable formalisation of this extended property.

1.2. Convergence to steady-state

The origin of the low Mach number preconditioning idea is related to the difficult issue for computing steady-states with wave speeds of very different size. A pseudo-unsteady iteration, inspired from the artificial compressibility method, and involving a pressure preconditioner was proposed by Turkel [16]. This work is at the origin of many pseudo-unsteady explicit algorithms for the computation of steady solutions.

Now, the Godunov method is very frequently combined with an implicit iteration using a "first-order Jacobian". Indeed, second-order Godunov approximations result in non-compact finite-difference molecules (let us say, with five diagonals in 1D), while the first-order Jacobian is compact (three diagonals in 1D). The preconditioning of a second-order accurate approximation by a first-order one has been studied and referred in the literature as the *first-order second-order defect-correction iteration*. A beautiful state of the art is proposed in [6]. In the case of transonic flows, the authors of that paper show that this iteration has rather good convergence properties. In the case of low Mach number flow, however, the convergence deteriorates dramatically. In this work, we give some arguments explaining this feature, and we show that the introduction of the low Mach preconditioner in the upwind stabilization term of both approximation and Jacobian cures this problem.

1.3. Time accuracy

The accuracy of a numerical approximation is above all determined by the amount of information devoted to the description of a given phenomenon.

In advection phenomena, not only the advected quantities have to be well described by the spatial mesh, but also the time step size has to be small accordingly; the limitation on the time step size for accuracy can be expressed by the Courant–Friedrichs–Lewy (CFL) condition (which is also a stability condition for explicit time advancing schemes). If we apply an implicit time advancing scheme, using larger time step will result in either Gibbs oscillations, or, if the numerical scheme has enough dissipation, in high dissipation errors. Such dissipative schemes are often first-order accurate ones. Moreover, even with high order accurate schemes, the practical accuracy may not be better that first-order when details are not captured. By "practical accuracy order", we mean the apparent order of accuracy for a given size of time step, by opposition to the formal order of accuracy, that is an asymptotic one i.e. applying only for "small enough", may be very small, time step. In the Navier–Stokes model for compressible fluids, both entropy waves and acoustics are advected. This seems to indicate that, for reasonable accuracy, a CFL condition relying on both fluid velocity and sound speed should be imposed. Conversely, implicit time advancing methods and large time steps would be applied only with an important dissipation for damping the too fast waves, that is with first-order practical accuracy. This remark is in fact not true for all kind of flows. Indeed, for a large class of compressible flows, the evolution of variables, the time derivative of which are computed by divided differences, is much slower than the travel of a high frequency wave at sound speed. Therefore, the underlying Taylor formula is accurate and high-order practical accuracy is obtained with large time steps. As examples of such fluid problems, we refer to flows with slow variation of geometry, such as in fluid-structure flutter analysis, and piston engines calculations; the domains of combustion and maybe of aeroacoustic coupling involve also many contexts of this type. In case of transonic flows, time accuracy is observed when the velocity of shocks are small enough. A special category is the case of low Mach and very low Mach flows. In the case where asymptotic models are very accurate, then implicit schemes (that are mandatory for these models) with high-order accuracy can be applied with benefit (large time steps, good accuracy) and result in higher efficiency. In the case where a complete compressible Navier–Stokes model is applied, the question of the efficiency of a strategy relying on large time steps and high-order accurate time advancing is open.

One purpose of this paper is to examine the use of a third-order accurate implicit scheme in a complete compressible Navier–Stokes model with some emphases on low Mach flows.

Third-order time accuracy is rarely implemented in complex CFD codes. Yet, third-order accuracy is accompanied with small phase errors for advection phenomena; then spurious oscillations are also reduced as compared with second-order accuracy.

Since direct methods are not applicable to complex CFD systems, iteration is the rule, and so we may consider nonlinear solvers at each time step. Then the two-stage scheme of Norsett [11] seems to be a convenient choice and we present its combination with the first-order Jacobian preconditioning.

1.4. Applications

Our study will cover a sample of steady applications involving some classical low Mach number flows and a non-classical one related to the thermics in a turbo-engine. An academic unsteady natural convection problem is also investigated from the point of view of acoustics progressive damping.

1.5. Plan

After a first section recalling some features of low Mach number asymptotics, we analyse the influence of the Turkel preconditioning in the Roe flux splitting in the context of these asymptotics. Then we analyse the efficiency of the defect-correction method with and without the preconditioning and give some steady-state applications. Finally the third-order accurate implicit time advancing scheme is described and applied to a complex transient problem.

The remaining part of this paper is organized as follows:

2. Low Mach asymptotics;
3. Low Mach Godunov-type method;
4. Analysis of the defect-correction iteration;
5. Accurate implicit time advancing;
6. Application to steady low Mach flows;
7. Application to a transient convection problem;
8. Concluding remarks.

2. Low Mach asymptotics

There is some consensus about the better efficiency of asymptotic models for a collection of special contexts, as compared to the complete compressible model. This is particularly true for natural convection flows, computed well, up to now, with the low Mach number asymptotic model, and for many low speed flows computed accurately with the incompressible model.

We want, however, to emphasize that an adequate numerical treatment of the full compressible model allows good answers not only for the existing asymptotic contexts, but also for some other physical contexts that are near the asymptotic ones and are not accurately handled by the asymptotic approach. This section recalls some details of the low Mach number model in a format making the sequel more easy to read.

2.1. Basic asymptotics

We start considering the usual compressible model in conservation form, with gravity terms

$$\frac{\partial \rho}{\partial t} + \nabla \cdot (\rho \mathbf{u}) = 0, \tag{0.a}$$

$$\frac{\partial \rho \mathbf{u}}{\partial t} + \nabla \cdot (\rho \mathbf{u} \otimes \mathbf{u}) = -\nabla p + \nabla \cdot \tau + \rho g \mathbf{e}_g, \tag{0.b}$$

$$\begin{aligned} &\frac{\partial \rho \left(\varepsilon + \frac{1}{2}\|\mathbf{u}\|^2\right)}{\partial t} + \nabla \cdot \left(\rho \mathbf{u}\left(\varepsilon + \frac{1}{2}\|\mathbf{u}\|^2\right)\right) \\ &\quad = -\nabla \cdot (p\mathbf{u}) + \nabla \cdot (\tau : \mathbf{u}) \\ &\qquad + \nabla \cdot (k \nabla T) + \rho g \mathbf{e}_g \cdot \mathbf{u} \end{aligned} \tag{0.c}$$

with

$$p = R\rho T, \tag{0.d}$$

$$\varepsilon = C_v T, \tag{0.e}$$

$$\tau = \mu\left(\nabla \mathbf{u} + (\nabla \mathbf{u})^{\mathrm{T}} - \frac{2}{3}(\nabla \cdot \mathbf{u})\mathbf{I}\right). \tag{0.f}$$

where ρ is the density, u_i the components of the velocity vector $\mathbf{u}$, g_i the components of the gravity acceleration $g\mathbf{e}_g$ and $\mathbf{e}_g$ is the unit vector giving the direction of gravity forces.

Then the equation of the total energy becomes:

$$\begin{aligned} &\rho C_p\left(\frac{\partial T}{\partial t} + u \cdot \nabla T\right) - \left(\frac{\partial P}{\partial t} + u \cdot \nabla P\right) \\ &\quad - \tau : \nabla u - \nabla \cdot (k \nabla T) = 0 \end{aligned} \tag{1}$$

using the momentum equation multiplied by the velocity. In the *standard low Mach number flow analysis* [13], the non-dimensionalisation allowing to keep a set of variables all of the order of unity introduces necessarily a new factor for the pressure term in moment equations. This factor often called the Euler number is the inverse of the square of a reference Mach number.

In our analysis, we conserve without any adimensional factor the Euler part of the Navier–Stokes equations i.e., we take the *Strouhal*, *Euler* and *Eckert* numbers equal to one and also

$$T_* = \varepsilon_* / C_v \tag{2}$$

as in most Navier–Stokes numerical solvers.

Then, either the velocity tends to zero, or the energy tends to infinity when the Mach will be made smaller and smaller. Our asymptotic *ansatz* on "non-dimensionalised" variables relies on the last option

$$\begin{aligned} \tilde{\rho} &= \tilde{\rho}_0 + M_* \tilde{\rho}_1 + M_*^2 \tilde{\rho}_2 + \cdots, \\ \tilde{\mathbf{u}} &= \tilde{\mathbf{u}}_0 + M_* \tilde{\mathbf{u}}_1 + M_*^2 \tilde{\mathbf{u}}_2 + \cdots, \\ \tilde{p} &= (1/M_*^2)\tilde{p}_0 + (1/M_*)\tilde{p}_1 + \tilde{p}_2 + \cdots, \\ \tilde{T} &= (1/M_*^2)\tilde{T}_0 + (1/M_*)\tilde{T}_1 + \tilde{T}_2 + \cdots. \end{aligned} \tag{3}$$

We assume that Reynolds and Froude numbers are much larger than the Mach number

$$\frac{M_*^2}{Re} \ll 1, \quad \frac{M_*^2}{Fr} \ll 1.$$

We recall that in the asymptotic model the three first unknowns converge to bounded values while it is the quotient of the fourth one by M_*^2 that converges to a bounded value.

It results that we can pass to the limit on the continuity equations with only bounded quantities and then the limit differential equation is unchanged.

The largest terms in the momentum equations give successively $\tilde{\nabla}\tilde{p}_0 = 0$ and $\tilde{\nabla}\tilde{p}_1 = 0$. *Assuming also that boundary conditions allow a uniform static pressure for the solution*, we deduce that $\tilde{p}_0$ and $\tilde{p}_1$ are uniform over the (connex) geometrical domain.

The bounded terms in the momentum equations couple the bounded density and momentum to the gradient of the zero-order term $\tilde{p}_2$ in the pressure asymptotic expansion.

For the sake of clarity, let us multiply the energy equation (1) by a M_*^2 factor before passing to the limit. The kinetic energy is two orders smaller and can be discarded from the energy equation, which then reduces essentially to the heat equation. The four limit equations

give us the so-called *low Mach or dilatable asymptotical model*

$$\frac{\partial\tilde{\rho}_0}{\partial\tilde{t}}+\tilde{\nabla}\cdot(\tilde{\rho}_0\tilde{\mathbf{u}}_0)=0, \tag{4.a}$$

$$\frac{\partial\tilde{\rho}_0\tilde{\mathbf{u}}_0}{\partial\tilde{t}}+\tilde{\nabla}\cdot(\tilde{\rho}_0\tilde{\mathbf{u}}_0\otimes\tilde{\mathbf{u}}_0)=-\tilde{\nabla}\tilde{p}_2+\frac{1}{Re}\tilde{\nabla}\cdot\tilde{\tau}_0+\frac{1}{Fr}\tilde{\rho}_0\mathbf{e}_g, \tag{4.b}$$

$$\tilde{\rho}_0\left(\frac{\partial\tilde{T}_0}{\partial\tilde{t}}+\tilde{\mathbf{u}}_0\cdot\tilde{\nabla}\tilde{T}_0\right)-\frac{1}{\gamma}\frac{\mathrm{d}\tilde{p}_0}{\mathrm{d}\tilde{t}}-\frac{1}{Pe}\tilde{\nabla}^2\tilde{T}_0=0, \tag{4.c}$$

$$\tilde{p}_0=(\gamma-1)\tilde{\rho}_0\tilde{T}_0, \tag{4.d}$$

where

$$\frac{\mathrm{d}(\cdot)}{\mathrm{d}\tilde{t}}=\frac{\partial(\cdot)}{\partial\tilde{t}}+\tilde{\mathbf{u}}_0\cdot\tilde{\nabla}(\cdot). \tag{5}$$

This model is very useful in several different fields of applications, and has been in particular much used for low Mach combustion flows.

An extension to real gas is possible. Let us assume that the state law is written

$$\mathrm{d}p=\xi\mathrm{d}\rho+\kappa\mathrm{d}\rho\varepsilon \tag{6}$$

with

$$\xi=\left(\frac{\partial p}{\partial\rho}\right)_{\rho\varepsilon},\quad \kappa=\left(\frac{\partial p}{\partial\rho\varepsilon}\right)_{\rho}.$$

Then Eq. (1) becomes

$$\frac{(\rho\xi+\kappa(\rho\varepsilon+p))}{\rho\xi}\frac{\mathrm{d}(\rho\varepsilon)}{\mathrm{d}t}-\frac{(\rho\varepsilon+p)}{\rho\xi}\frac{\mathrm{d}p}{\mathrm{d}t}-\tau:\nabla u-\nabla\cdot(k\nabla T)=0. \tag{7}$$

The equations are non-dimensionalised as in the case of a perfect gas except that now we take $T_*=\varepsilon_*$, and also $\xi_*=\varepsilon_*$, $\kappa_*=1$. In addition to the asymptotic development (cf. (3)), we take

$$\begin{aligned}\tilde{\rho}\tilde{\varepsilon}&=\frac{1}{\tilde{M}_*^2}(\tilde{\rho}\tilde{\varepsilon})_0+\frac{1}{\tilde{M}_*}(\tilde{\rho}\tilde{\varepsilon})_1+(\tilde{\rho}\tilde{\varepsilon})_2+\cdots,\\ \tilde{\xi}&=\frac{1}{\tilde{M}_*^2}\tilde{\xi}_0+\frac{1}{\tilde{M}_*}\tilde{\xi}_1+\tilde{\xi}_2+\cdots,\\ \tilde{\kappa}&=\tilde{\kappa}_0+\tilde{M}_*\tilde{\kappa}_1+\tilde{M}_*^2\tilde{\kappa}_2+\cdots.\end{aligned} \tag{8}$$

Then we obtain a dilatable-like model composed of Eqs. (4.a) and (4.b) together with

$$\frac{(\tilde{\rho}_0\tilde{\xi}_0+\tilde{\kappa}_0((\tilde{\rho}\tilde{\varepsilon})_0+\tilde{p}_0))}{\tilde{\rho}_0\tilde{\xi}_0}\frac{\mathrm{d}(\tilde{\rho}\tilde{\varepsilon})_0}{\mathrm{d}\tilde{t}}-\frac{((\tilde{\rho}\tilde{\varepsilon})_0+\tilde{p}_0)}{\tilde{\rho}_0\tilde{\xi}_0}\frac{\mathrm{d}\tilde{p}_0}{\mathrm{d}\tilde{t}}-\frac{1}{Re}\tilde{\tau}_0:\tilde{\nabla}\tilde{u}_0-\frac{1}{Pe}\tilde{\nabla}\cdot(\tilde{k}\tilde{\nabla}\tilde{T}_0)=0, \tag{9}$$

where

$$\mathrm{d}\tilde{p}_0=\tilde{\xi}_0\mathrm{d}\tilde{\rho}_0+\tilde{\kappa}_0\mathrm{d}(\tilde{\rho}\tilde{\varepsilon})_0. \tag{10}$$

This model is also applicable to certain types of two-phase flows. We refer to [2,21] for low Mach number diphasic flows.

Let us recall that for small temperature amplitudes, a constant density approximation can be applied in the continuity equation and the model (9) can be replaced by the *Boussinesq model*, which, in turn, under an isothermal assumption would reduce to the *incompressible model*.

2.2. Taking into account a pressure gradient

In an important class of applications, we do not wish to assume that boundary conditions allow a uniform static pressure. This is the case when gravity terms are accounted for, so that the pressure involves an hydrostatic component. We shall need in the sequel to consider the following conditions:

In a part of the boundary, the static pressure is

$$\tilde{p}=\tilde{p}_0-kM_*^2\tilde{p}_0 \tag{11}$$

and in the other part:

$$\tilde{p}=\tilde{p}_0+kM_*^2\tilde{p}_0 \tag{12}$$

where k does not depend on M_*.

Then the asymptotical analysis gives again a "dilatable" limit, and (11) and (12) give boundary conditions for the second-order pressure fluctuation $\tilde{p}_4$, respectively:

$$\tilde{p}_4=-k\tilde{p}_0\quad\text{or}\quad+k\tilde{p}_0 \tag{13}$$

to be combined with Eq. (9). We shall give an example of such a flow in Section 6.2.

3. Low Mach Godunov-type method

3.1. Central differencing

Let us write a vertex-centered central differenced finite volume scheme for the Euler equations applied to an unstructured mesh as follows:

$$\mathbf{\Psi}_h(\gamma,W)_j=\sum_{k\in V(j)}\Phi^{\text{central}}(W_j,W_k,\vec{\eta}_{jk})+\mathbf{B}_h(\gamma,W)_j, \tag{14}$$

where $V(j)$ is the set of vertices that are neighbors of j, $\vec{\eta}_{jk}$ is the integral on interface between j and k of the normal vector. Symbol $\mathbf{B}_h(\gamma,W)_j$ holds for boundary fluxes. The centered integration for elementary flux Φ is written as follows:

$$\Phi^{\text{central}}(W_j,W_k,\vec{\eta}_{jk})=0.5(F_j+F_k)\cdot\vec{\eta}_{jk}, \tag{15}$$

where $F_j=F(W_j)$ are the Euler fluxes computed at W_j. This is equivalent in introducing the following discrete space operator ∇_h:

$$\nabla_h(f)_j = \sum_{k\in V(j)} (f_j + f_k)/2\vec{\eta}_{jk}/\mathrm{area}(j), \tag{16}$$

where area(j) is the cell area.

Let us assume that the above asymptotic expansion applies to a discrete solution family. Due to the fact that ∇_h depends neither on M_* nor the dependent flow variables W, this operator commutes with the asymptotic expansion. For example, the Euler fluxes satisfy the following estimate:

$$\left(\frac{\partial F}{\partial W}\right)_1 \sim \begin{bmatrix} 0 & \mathrm{O}(1) & 0 & 0 \\ \mathrm{O}(1) & \mathrm{O}(1) & \mathrm{O}(1) & \mathrm{O}(1) \\ \mathrm{O}(1) & \mathrm{O}(1) & \mathrm{O}(1) & 0 \\ \mathrm{O}\left(\frac{1}{M_*^2}\right) & \mathrm{O}\left(\frac{1}{M_*^2}\right) & \mathrm{O}(1) & \mathrm{O}(1) \end{bmatrix}. \tag{17}$$

Then it remains to multiply the last equation by M_*^2 for obtaining the discrete low Mach limiting equations, similarly to the continuous case.

Unfortunately, we cannot make the discretization parameter h tend to the limit, since the proposed central differenced approximation is not stable (and not convergent in practice). This difficulty is often solved by applying Godunov differencing.

3.2. Godunov differencing

Godunov-type methods rely on discontinuous representations of the unknown and computation of fluxes at discontinuities in function of both "left" and "right" values by applying an approximate or an exact Riemann solver. This process introduces numerical viscosity terms that are very useful for stabilizing transonic flows.

Let us write a vertex-centered first-order Godunov scheme for the Euler equations applied to an unstructured mesh as follows:

$$\mathbf{\Psi}_h(\gamma, W)_j = \sum_{k\in V(j)} \Phi(W_j, W_k, \vec{\eta}_{jk}) + \mathbf{B}_h(\gamma, W)_j, \tag{18}$$

where $V(j)$ is the set of vertices that are neighbors of j, $\vec{\eta}_{jk}$ is the integral on interface between j and k of the normal vector. Symbol $\mathbf{B}_h(\gamma, W)_j$ holds for boundary fluxes. The upwinding in elementary flux Φ is the Roe flux splitting. In the case of the standard Roe splitting, we have

$$\Phi(W_j, W_k, \vec{\eta}_{jk}) = 0.5(F_j + F_k)\cdot\vec{\eta}_{jk} + 0.5|\mathscr{A}|(W_j - W_k), \tag{19}$$

where $F_j = F(W_j)$ is the Euler flux computed at W_j, and $|\mathscr{A}|$ is the absolute value of the Jacobian flux along $\vec{\eta}_{jk}$

$$\begin{aligned} &\mathscr{A} = \left(\frac{\partial F}{\partial W}\right)_1 (\eta_{jk})_1 + \left(\frac{\partial F}{\partial W}\right)_2 (\eta_{jk})_2 \\ &\mathscr{A} = T\Lambda T^{-1}, \quad \Lambda \text{ diagonal}, \\ &|\mathscr{A}| = T|\Lambda|T^{-1}. \end{aligned} \tag{20}$$

These matrices are computed at an intermediate value $\overline{W}_{jk}$ of W [23].

The introduction of Turkel's preconditioner leads to the following *preconditioned* flux discretisation

$$\begin{aligned} \Phi(W_j, W_k, \vec{\eta}_{jk}) = {} & 0.5(F_j + F_k).\vec{\eta}_{jk} \\ & + 0.5P(M_*)^{-1}|P(M_*).\mathscr{A}|(W_j - W_k). \end{aligned} \tag{21}$$

The preconditioner $P(M_*)$ is a 4×4 matrix in 2D. The option that we consider was proposed by Turkel in [16]. It has been analysed for example in [10].

In term of the "primitive" variables $U = [p, u, v, ln(p/(\rho^\gamma))]$, this preconditioner writes:

$$P_U(\beta) = \begin{pmatrix} \beta^2 & 0 & 0 & 0 \\ 0 & 1 & 0 & 0 \\ 0 & 0 & 1 & 0 \\ 0 & 0 & 0 & 1 \end{pmatrix}.$$

In our study, the parameter β will be systematically chosen equal to the *reference Mach number* M^*.

For the conservative variables $W = [\rho, \rho u, \rho v, \rho e]$ the corresponding form is

$$P(M^*) = \frac{\partial W}{\partial U} P_U(M^*) \frac{\partial U}{\partial W}.$$

By tedious calculations we can analyse the behavior of the Roe scheme in the case of the convergence to a low Mach limit. The discretization now does not commute with the asymptotic expansion and a step by step calculation is necessary.

From this analysis it turns that the standard Roe viscosity (corresponding to $\beta = 1$) shows a spurious asymptotic behaviour. Indeed, when Mach number tends to zero, some terms become much larger than the consistent central-differenced fluxes. The fact that some other ones are too small can also produce unfavourable oscillations (only the analysis of fluxes in x direction—indicated by subscript 1—are presented here).

$$\left|\left(\frac{\partial F}{\partial W}\right)_1\right| \sim \begin{bmatrix} \mathrm{O}(1) & \mathrm{O}(M_*) & \mathrm{O}(M_*) & \mathrm{O}(M_*) \\ \mathrm{O}\left(\frac{1}{M_*}\right) & \mathrm{O}\left(\frac{1}{M_*}\right) & \mathrm{O}(M_*) & \mathrm{O}(M_*) \\ \mathrm{O}(M_*) & \mathrm{O}(M_*) & \mathrm{O}(1) & \mathrm{O}(M_*) \\ \mathrm{O}\left(\frac{1}{M_*}\right) & \mathrm{O}\left(\frac{1}{M_*}\right) & \mathrm{O}\left(\frac{1}{M_*}\right) & \mathrm{O}\left(\frac{1}{M_*}\right) \end{bmatrix}, \tag{22}$$

conversely, the preconditioned viscous term ($\beta = M_*$) shows a more regular behavior:

$$\begin{aligned} &P(M_*)^{-1}\left|P(M_*)\left(\frac{\partial F}{\partial W}\right)_1\right| \\ &\quad \sim \begin{bmatrix} \mathrm{O}(1) & \mathrm{O}(1) & \mathrm{O}(1) & \mathrm{O}(1) \\ \mathrm{O}(1) & \mathrm{O}(1) & \mathrm{O}(1) & \mathrm{O}(1) \\ \mathrm{O}(1) & \mathrm{O}(1) & \mathrm{O}(1) & \mathrm{O}(1) \\ \mathrm{O}\left(\frac{1}{M_*^2}\right) & \mathrm{O}\left(\frac{1}{M_*^2}\right) & \mathrm{O}\left(\frac{1}{M_*^2}\right) & \mathrm{O}\left(\frac{1}{M_*^2}\right) \end{bmatrix} \end{aligned} \tag{23}$$

that is coherent with the behavior of the Euler fluxes (17).

Similar behaviors are obtained for $(\partial F/\partial W)_2$ so that similar results hold for the whole stabilisation term $P(M_*)^{-1}|P(M_*)\mathscr{A}|$. Multiplying the energy equation by M_*^2 would complete the obtention of the low Mach discrete system.

As a consequence, the analysis can be transposed to the discrete context when the Turkel preconditioner is introduced in the stabilization term. This analysis shows the following *property*:

Property 1. *The usual Roe scheme, although a consistent scheme, presents a defavorable error behavior for low Mach flow. Conversely this kind of flow, including thermics, can be computed with the Turkel preconditioned version of Roe scheme with a Mach independent accuracy.*

Since only the spatial stabilization term is modified by the preconditioner and not the time derivative, we have also the following *property*:

Property 2. *Our analysis applies also to the unsteady case.*

Remark. In practice, the Turkel preconditioner has to be also introduced in any upwind boundary condition.

Before illustrating the impact of this *Property* on low Mach flows, we shall examine a second crucial issue, the convergence of a popular Newton-like iteration.

4. Analysis of the defect-correction iteration

We are interested in some implicit time stepping methods using the Roe scheme. These methods, referred to as Implicit or Linear defect-correction (LDC) methods, combine a second-order accurate spatial approximation with a first-order linear spatial operator and have been analysed in detail in [6].

The LDC method can be written as

$$\left(\frac{M}{\Delta t}+A_1(W^n)\right)(W^{n+1}-W^n)=-\Psi_2(W^n), \tag{24}$$

where M is the mass matrix, Δt is the time step. Symbol A_1 holds for an approximation of the Jacobian of the first-order accurate numerical flux (18). Symbol Ψ_2 holds for the second-order accurate (in space) numerical flux. We give now some informations about this approximation. It is an edge-based approximation, so that for each vertex j, the fluxes are computed with any neighboring vertex k ($k \in V(j)$). The novelty with respect to the first-order spatial accurate discretization is that the flow variables evaluations W_{jk} and W_{kj} used in the Roe approximate Riemann solver are derived from an higher-order interpolation

$$\mathbf{\Psi}_h(\gamma,W)_j=\sum_{k\in V(j)}\Phi(W_{jk},W_{kj},\vec{\eta}_{jk})+\mathbf{B}_h(\gamma,W)_j, \tag{25}$$

where the W_{jk} and W_{kj} are extrapolated according to the MUSCL method of Van Leer [19] extended to triangles as in [7]. In short

$$W_{jk}=W_j+\frac{1-\kappa}{2}(W_k-W_j)+\frac{\kappa}{2}(\nabla W)_j\cdot\overrightarrow{jk}, \tag{26}$$

where $(\nabla W)_j$ is a mean of the gradients of W on triangles around vertex j and κ is an upwind bias coefficient generally taken to $1/2$.

We restrict now our analysis to *scalar advection*, and in order to modelize the asymptotic behaviors (22) and (23), we consider an upwind viscosity term weighted with a parameter ζ:

$$\Phi(Q_j,Q_k)=\vec{a}\cdot\vec{\eta}_{jk}\frac{Q_j+Q_k}{2}+\frac{1}{2}\zeta\mid\vec{a}\cdot\vec{\eta}_{jk}\mid(Q_j-Q_k), \tag{27}$$

where $\vec{a}$ is the advective velocity. According to (22) and (23) the Roe scheme is modelized by (27) with $\zeta=\mathrm{O}(1/M_*)$ and with $\zeta=\mathrm{O}(M_*)$, and the preconditioned scheme is modelized by (27) with $\zeta=\mathrm{O}(1)$. The second-order accurate part is parameterized accordingly

$$\Phi(Q_{jk},Q_{kj})=\vec{a}.\vec{\eta}_{jk}\frac{Q_{jk}+Q_{kj}}{2}+\frac{1}{2}\zeta|\vec{a}.\vec{\eta}_{jk}\mid(Q_{jk}-Q_{kj}), \tag{28}$$

A 1D Fourier analysis applied only to LDC iteration with model (27) is sufficient for detecting the problems arising from an upwinding weight ζ too different from unity. Indeed, we can predict, see Fig. 1, the amplification factor of the LDC as a function of (a) the upwind bias coefficient κ and (b) the upwinding weight ζ. It was observed by Desideri and Hemker [6] that the best value of κ was 0.5. Fig. 1 gives an evidence of this. It also shows that the best value of ζ is one, and that the convergence fastly degrades when ζ deviates from one. It is then clear that our model shows the following behaviour:

Property 3. *In the context of the proposed* 1*D model, the implicit defect-correction schemes built with* (27) *have a convergence ratio which is mesh independent and which depends only on* ζ. *It degrades to* 1 *as* ζ *increases infinitely and can be larger than one when* ζ *is small.*

Our model then predicts that the convergence of the LDC scheme with low Mach number preconditioner in both second-order approximation scheme and first-order Jacobian would be independent of the Mach number whilst that of LDC with the Roe scheme (again for both

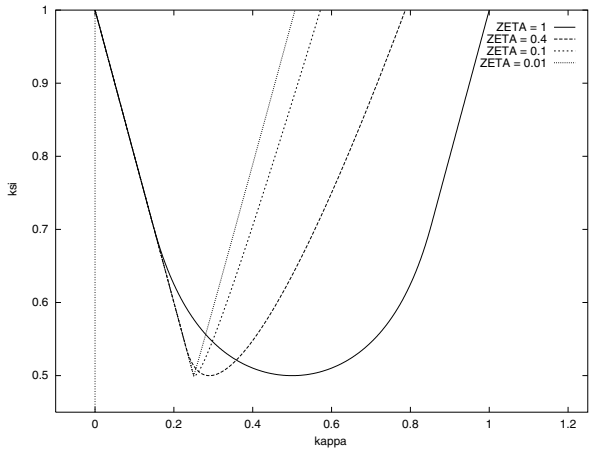

Fig. 1. Amplification factor (ordinate) of the LDC method as a function of the upwind bias coefficient κ (abscissa), obtained for different values of the upwinding weight ζ: when the weight ζ gets more different from 1, the amplification factor degrades towards 1.

second-order approximation scheme and first-order Jacobian) would be dependent of it. More details can be found in [20].

5. Accurate implicit time advancing scheme

Since the preconditioner is introduced only in the upwind viscosity term, the scheme is not only spatially consistent, but also can be advanced in time with time accuracy.

5.1. Linearised scheme with first-order accuracy in space

The hybrid order one/order two scheme used in Section 4 for calculating steady states can be extended to a first-order consistent time advancing

$$(M + \Delta t A_1^n)(W^{n+1} - W^n) = -\Psi_2(W^n), \tag{29}$$

where the linear operator A_1^n is the sum of a genuine Jacobian for the viscous fluxes and a first-order (in space) approximate Jacobian for the Euler fluxes

$$A_1^n = \left[\frac{\partial \Psi_1^{\text{inviscid}}}{\partial W} + \frac{\partial \Psi_2^{\text{viscous}}}{\partial W}\right](W^n).$$

At each iteration, the linear system is actually solved by a multigrid scheme described in [8] or by an LU factorization method. For unsteady laminar flows, the accuracy of the above scheme turns to be of $O(\Delta t, \Delta t \Delta x, \Delta x^2)$, which in practice is not much accurate and limits the size of time steps usuable for a given accuracy.

5.2. An implicit Runge–Kutta scheme

Second-order accuracy in time is easily obtained with the extension BDF2 relying on the second-order difference in time:

$$\frac{\partial W}{\partial t} = \lambda_1 W^{n+1} + \lambda_0 W^n + \lambda_{-1} W^{n-1} + O(\Delta t^2) \tag{30}$$

with $\lambda_1 = 3/(2\Delta t)$, $\lambda_0 = -2/\Delta t$ and $\lambda_{-1} = 1/(2\Delta t)$.

This scheme will produce an unconditionally stable scheme for both advection and diffusion. In [14] is presented a combination of Eq. (30) with defect-correction. On the contrary, BDF3 is unconditionally stable only for diffusion operators.

To build a higher-order accurate scheme, we have chosen a nonlinear scheme with two implicit systems to solve at each iteration, the singly diagonal two-stage implicit Runge–Kutta (SDIRK) scheme of Norsett [11]:

$$\begin{aligned}
\delta\overline{W_1} &= -\Psi(W^n + \Delta t(a_{11}\delta\overline{W_1} + a_{12}\delta\overline{W_2})),\\
\delta\overline{W_2} &= -\Psi(W^n + \Delta t(a_{21}\delta\overline{W_1} + a_{22}\delta\overline{W_2})),\\
W^{n+1} &= W^n + \Delta t(b_1\delta\overline{W_1} + b_2\delta\overline{W_2})
\end{aligned} \tag{31}$$

with

$$\begin{aligned}
&b_1 = 1/2, \quad b_2 = 1/2,\\
&a_{11} = \frac{3+\sqrt{3}}{6}, \quad a_{21} = 1 - 2a_{11}, \quad a_{22} = a_{11}, \quad a_{12} = 0.
\end{aligned} \tag{32}$$

It is known that the above scheme is third-order accurate in time, unconditionally stable for any complex gain coefficient of nonnegative real part ($A-(\frac{\pi}{2})$ stability), which ensures stability for both advection and diffusion processes.

At each stage of the SDIRK scheme, a nonlinear system has to be solved. We solve it by two nested loops. First a Newton-like or defect-correction iteration is preconditioned by the above first-order (in space) simplified linearised system, we perform a number α of defect-correction iterations. Second, the linearised system is solved by a multi-grid cycling or a direct factorization method.

6. Application to steady low mach flows

The following computations are presented in order to illustrate and hopefully confirm the properties arising from the theoretical part of this paper. We start with some classical incompressible and low Mach flows, then we present a case that should not be computed with an asymptotical model. In any case, it is either necessary or useful to identify the reference Mach number for understanding the asymptotic behaviour of the solution and use this information in the numerical model.

6.1. Spatial accuracy evaluation (1): lid driven cavity

It is not useless to illustrate that the "preconditioned-compressible" technology presented in this study can compete from an *accuracy* standpoint (i.e. with a comparable number of degrees of freedom) with some classical technology available for incompressible flows. We consider the lid-driven cavity for an incompressible flow, Reynolds number of which is 1000. A well-known reference computation has been performed by Ghia et al. [9] with a central-differenced second-order approximation and a fine cartesian mesh with 129×129 nodes. But the interest of this test case is that a *very accurate* solution is available. Indeed, Botella and Peyret [1] have applied a Chebyshev spectral approximation with singular basis functions for the corners; their computation allows an accuracy of 10^{-5}–10^{-6}.

In our compressible calculation, we need to identify an evolutive process with an initial condition. This allows to define a reference Mach number M_* as the ratio of the lid velocity to the uniform sound velocity in the initial stagnating atmosphere in the box:

$$M_* = \frac{\|\mathbf{u}^{\text{lid}}_{\max}\|}{a^{\text{init}}}. \tag{33}$$

When M_* is large, the compressible solution can deviate from the incompressible one. We can manage to obtain such a model error not larger than 10^{-6}. Indeed, the deviation between incompressible and compressible varies as the square of the Mach number; it is enough in our case to specify a Mach number of 10^{-3}. The grids that are used are chosen cartesian, for the sake of comparison, with 41×41, 81×81 and 161×161 nodes.

In Fig. 2 we present some horizontal cuts of the vertical velocity. The observation of these curves seems to indicate a reduction factor of the deviation between two solutions better than four, that is a numerical convergence order better than two.

Of course, for the same number of nodes, the best incompressible scheme is likely one order of magnitude faster than the proposed method; but if both calculations are affordable, the user can be interested in applying a unique method for a very large family of flows.

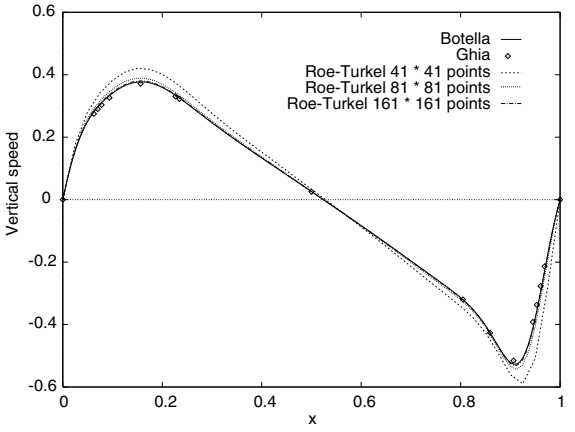

Fig. 2. Horizontal cut of vertical velocity for the lid-driven cavity test with $M_* = 10^{-3}$ and $Re = 1000$. Continuous line gives the very accurate reference result of Botella and Peyret, lozenges are results from Ghia et al. with a 129×129 mesh, dashes correspond to the results obtained with the presented method for three different meshes: 41×41, 81×81 and 161×161.

6.2. Spatial accuracy evaluation (2): natural convection

We turn now to a flow with heat transfer. Real life problems of this type are generally *not* steady. We start with a steady case and a first remark on the conditions of application of the proposed method, then we will come back to this context in the last section for the unsteady variant. Natural convection problems have been studied during decades with the Boussinesq model. This model not only assumes an incompressible flow but also a small variation of temperature. A very classical test case for *steady* natural convection was defined by De Vahl Davis in [3]. With the compressible approach, we have to handle an extra parameter, a Mach number that is representative of the flow. We define it as follows:

$$(M_*)^2 = \frac{\Delta T g l}{\gamma R (T_{\text{mean}})^2}, \tag{34}$$

where g is the gravity acceleration, l the size of the box, R the usual perfect gas constant, γ the usual ratio of calorific constants. ΔT is the difference of temperature between the cold and the warm walls, and T_{mean} is the arithmetic mean between these two temperatures.

It is possible to compute accurately this case with the method described in this study. However, a difficulty that we have encountered is the following one: in the compressible case the physical conditions of the problem involve total mass and energy. This should be adequately prescribed in the initial conditions and strictly preserved during the (pseudo-)unsteady calculation. Transient conservation is in fact satisfied if the linear systems with first-order Jacobian in the time-advancing

scheme are perfectly solved (in contrast to a rough iterative convergence). For very low Mach number, only the application of a direct solver could produce reliable results, i.e. results of best accuracy, which does not dependent of the transient history. We present in Fig. 3 a few results in order to illustrate that this is easily calculated with a coarse mesh (cartesian, 41×41). The Nusselt number is captured with less than 5% deviation compared to the Vahl Davis [3] results. This short example confirms the accuracy statement of Property 1 in the case where thermics are computed. We shall return to this physical context in Section 7.1.

6.3. Defect-correction convergence: airfoil flow

For illustrating the iterative properties of the defect-correction iteration, we consider the very simple steady Euler flow around a NACA0012 airfoil (with zero angle of attack; the definition of this airfoil can be found for example in [5]). We consider three different values of the farfield Mach number, $M_\infty = 0.1, 0.01, 0.001$ that plays the role of the reference Mach number M_*. The above implicit scheme is applied with large time steps, which are taken proportional to the inverse of the farfield Mach number. In the case of the Roe scheme, see Fig. 4(top), the convergence considerably degrades for lower Mach numbers, while the same LDC iteration for the scheme with "preconditioned" upwind vicosity, see Fig. 4(bottom), shows a convergence that is essentially Mach number independent, in accordance with Property 3 in Section 4.

6.4. An example not solved by asymptotic models

The fact that the dilatable model is often called "the low Mach model" can be interpreted as the tendancy of engineers to estimate most low Mach flows as dilatable ones at the asymptotic limit. The proposed example shows a counter example.

Turbo-engines combustion chambers are limited by metallic walls with a large number of small perforations. These perforations allow an external colder flow to get

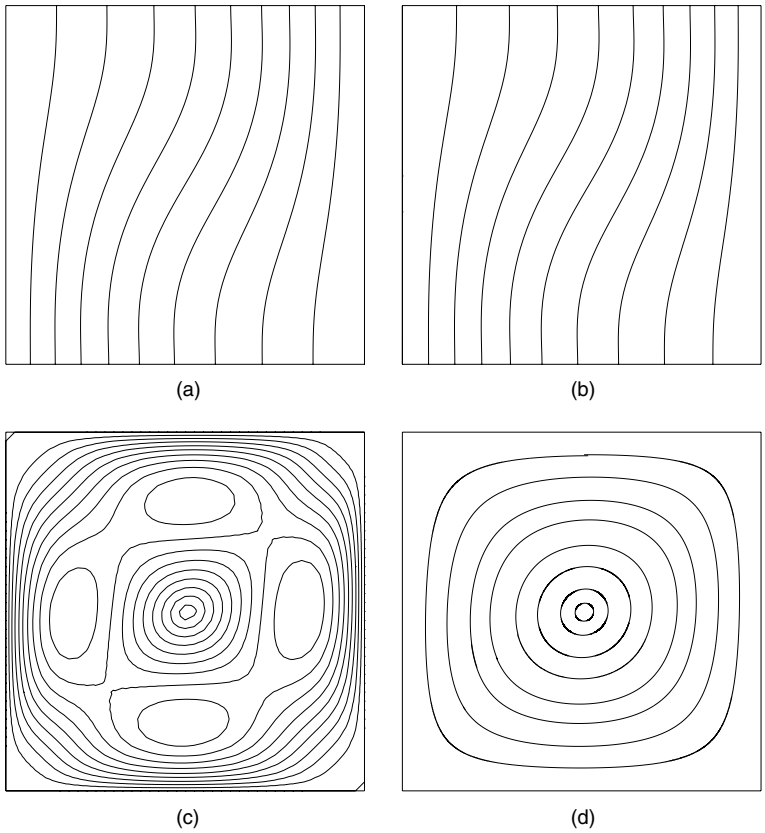

Fig. 3. Natural convection square box ($Pr = 0.71$, $\gamma = 1.4$, $\epsilon_* = \frac{\Delta T}{2T_{\text{mean}}} \simeq 0.07322$, $M_* = 10^{-4}$, Rayleigh number $Ra = 10^3$): (a) temperature contours (from 263.15 to 285.15 K, $\Delta T = 2$ K); (b) density contours (from 1.11874 to 1.20377 kg/m^3, 10 intervals); (c) Mach number contours (from 0 to 1.36365×10^{-5}, 10 intervals); (d) streamlines.

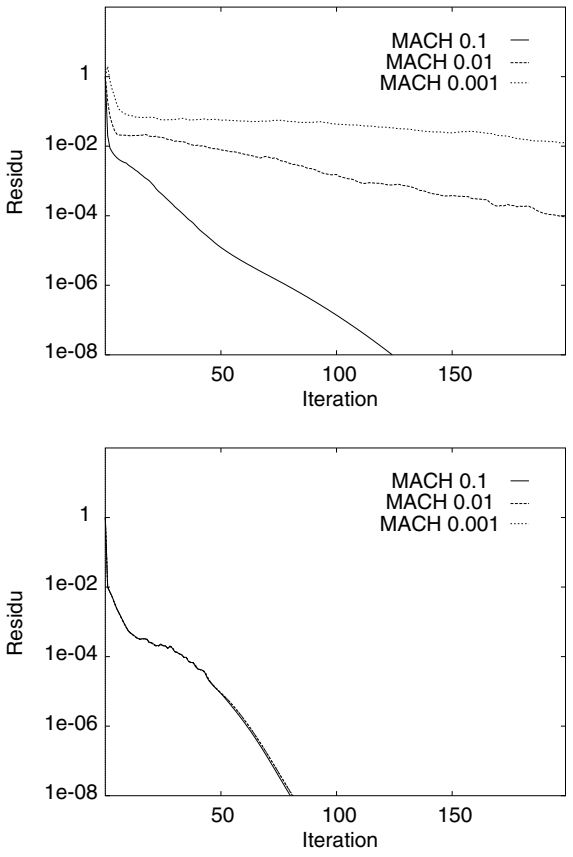

Fig. 4. Evolution of the normalized residual (ordinate) with time iterations (abscissa). Convergence of the non linear time stepping (inner linear relaxation is converged) for an implicit defect-correction method with the usual Roe scheme, that is without a preconditioner in the viscous term (top) and with a Turkel preconditioner in the viscous term (bottom).

in and help a colder boundary layer to protect the wall against too high heat. The way only one hole interfers with internal and external flows is difficult to compute.

Indeed the flow is a low Mach flow (Mach is about a few thousandths), but asymptotic models should not be used since the size of fluctuations of pressure, density and temperature are forced by the differences between external and internal flows.

Another important difficulty that we shall not address here is the fact that the size of the hole, smaller than the turbulent boundary layer thickness, induces important local laminar behaviors. In the present study, we restrict to a laminar model. We shall just give with Fig. 5 a rough idea of the flow: the upper (turbulent) boundary layer disappears at hole location due to suction, the lower boundary layer is not much affected. A mesh of 16,000 nodes was necessary for this computation.

The boundary conditions specify some uniform pressures at farfield, with two different values at upper

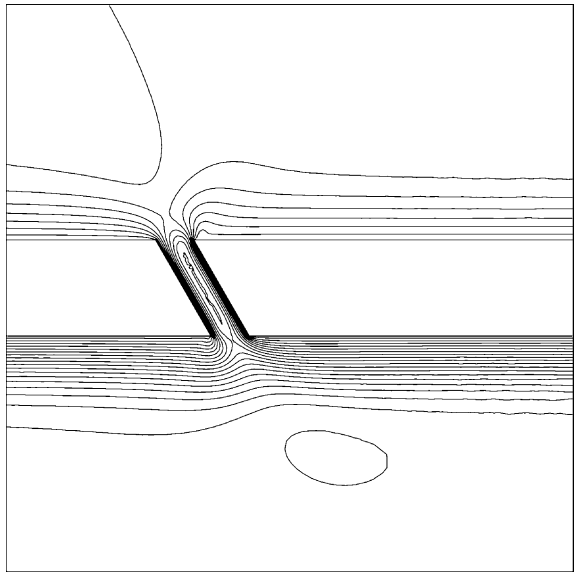

Fig. 5. Low Mach flow near a perforated wall: contours of the module of velocity, from 0 to 3 m/s. External flow is on upper side, with a smaller mean velocity, and a higher pressure; both flows go from left to right. In this first computation, mean temperatures of the two flows are identical.

and lower parts of the geometry. The velocities are on each part set equal to (2.74, 0) at farfield.

Furthermore, the wall condition is an isothermal one, with the same prescribed temperature for both sides of the wall.

If we neglect the heat fluxes at the walls, that is if we assume an adiabatic condition, then we can apply the asymptotic model proposed in Section 2 and use a "dilatable" CFD kernel with prescribed pressure. In order to illustrate this assertion, we have computed two self-similar solutions according to the analysis:

In Computation 1, the Mach numbers at farfield are, respectively, 2.9×10^{-3} (upper side) and 8×10^{-3} (lower side) The velocities at farfield are 10.1 (upper) and 27.5 (lower). The Reynolds is 700. (with respect to hole section).

In Computation 2, all above figures are kept except the Mach number: 2.9×10^{-2} (upper side) and 8×10^{-2} (lower side).

We observe that our flows are nearly self-similar for velocity and for pressure, see Figs. 6 and 7 for the velocity and, see Figs. 8 and 9 for the pressure.

However the pressure is not uniform, according to our asymptotic model. As a result, the density and temperature contours have not to be similar between the two computations, since ρT is not constant. Indeed the similarity is not good for temperature (Figs. 12 and 13) and density (Figs. 10 and 11) between the two computations.

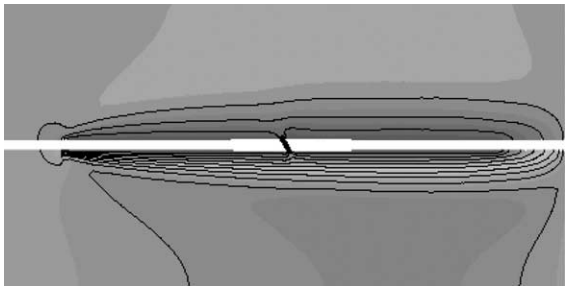

Fig. 6. Low Mach flow near a perforated wall: Computation 1; contours of the modulus of velocity, from 0 to 32 m/s.

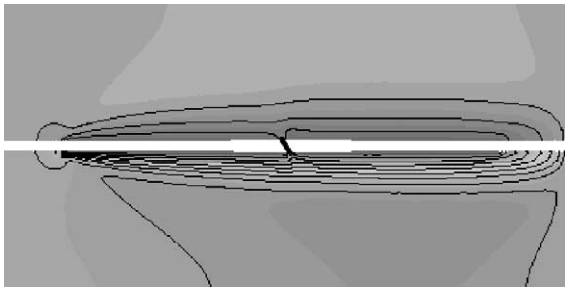

Fig. 7. Low Mach flow near a perforated wall: Computation 2; contours of the modulus of velocity, from 0 to 32 m/s.

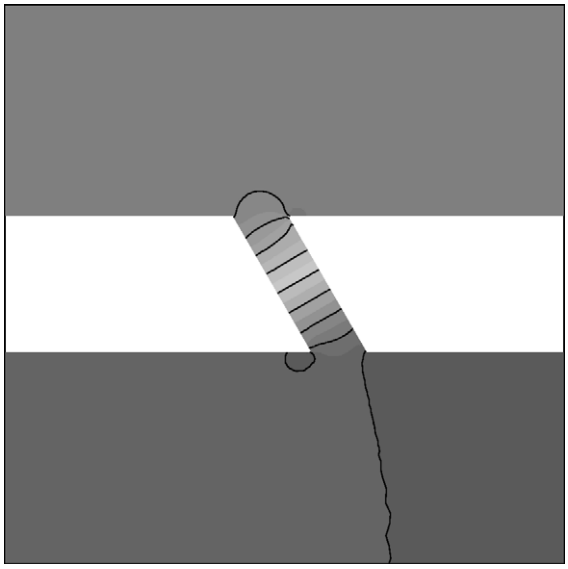

Fig. 8. Low Mach flow near a perforated wall: Computation 1; contours of the pressure, from 10129000 to 10133000 Pa.

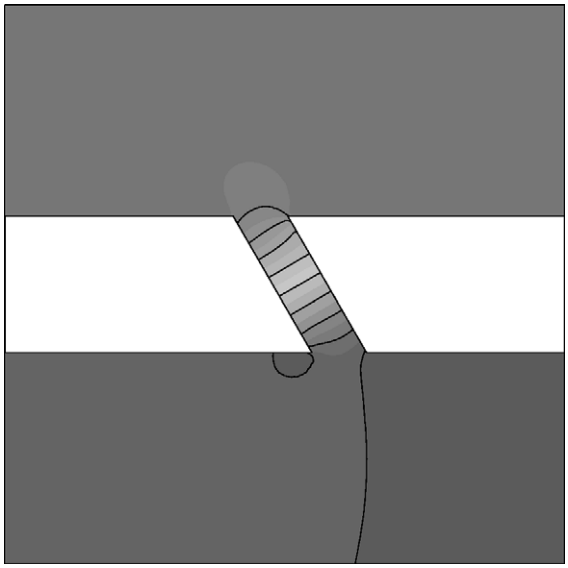

Fig. 9. Low Mach flow near a perforated wall: Computation 2; contours of the pressure, from 97960 to 101410 Pa.

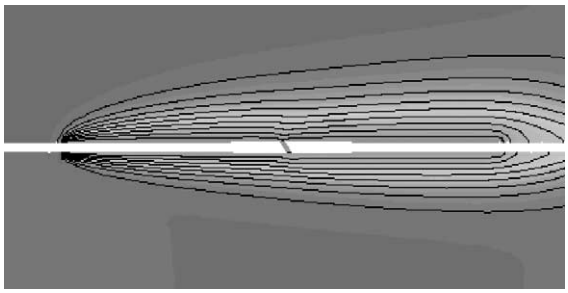

Fig. 10. Low Mach flow near a perforated wall: Computation 1; contours of density, from 1.9987 to 1.20333 kg/m^3.

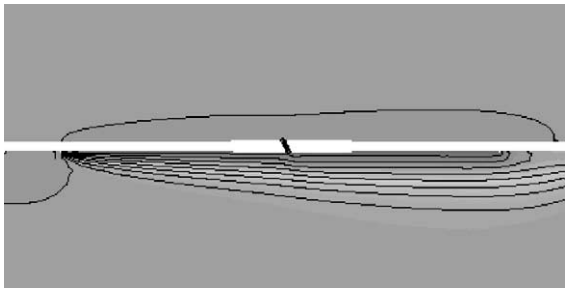

Fig. 11. Low Mach flow near a perforated wall: Computation 2; contours of density, from 1.16515 to 1.20482 kg/m^3.

This discrepancy in similarity is explained by the fact that the asymptotic analysis cannot take into account an isothermal condition.

This illustrates that the flow under analysis does not perfectly satisfy the assumptions of the asymptotic limit, and shows that the use of a dilatable model for the

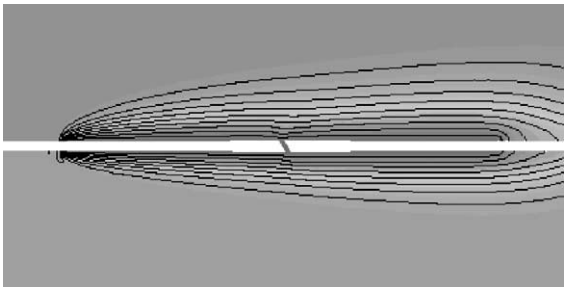

Fig. 12. Low Mach flow near a perforated wall: Computation 1; contours of temperature, from 29320.2 to 29401.7 K.

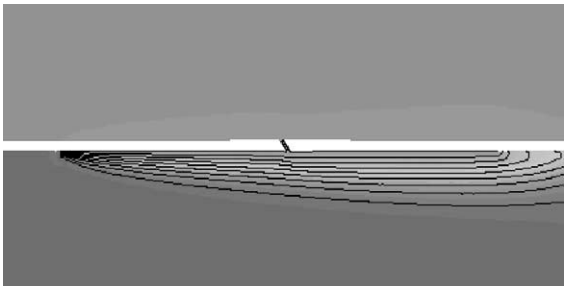

Fig. 13. Low Mach flow near a perforated wall: Computation 2; contours of temperature, from 285.021 to 294.032 K.

calculation would introduce a notable error. This kind of flow perfectly justifies the use of the compressible methods presented in this paper.

In the near future, we wish to compute a turbulent case. The Reynolds will not be so large close to the perforation, relaminarisation will happen and this is a motivation for applying an *unsteady* LES study. Then we need an implicit and accurate time advancing scheme as developed in the previous section and experimented in the next section.

7. Application to a transient convection problem

7.1. Definition of the transient problem

In many transient flows of industrial interest, the Mach number is not so large, but the actual transient phenomena cover the different time scales of that kind of flow, i.e. the acoustic scale, very fast, and other scales related to convection. Asymptotic models are by definition unable to account for the acoustic waves. In a preliminary study of this kind of flow, we consider a transient version of the convection box of De Vahl Davis (previous section). It is built by specifying an initial condition: the fluid in the square cavity is at rest with uniform temperature equal to the (right horizontal) cold wall. Evolution will be forced by putting suddenly the temperature of the left vertical wall to a larger level and maintaining it at this level (warm wall temperature). After fast acoustic phenomena, convection settles down and progressively gets steady, see Fig. 14. The Mach number in this case is of the order of 10^{-4}. In the present study, we conserve the spatial discretization conditions presented in Section 6.2, that is a second-order spatial scheme, and a rather coarse mesh with 41×41 nodes.

7.2. Adaptive time stepping

Since both time advancing schemes are a priori unconditionally stable, time steps as large as we want can be used. But accuracy can be a mess. In case of scheme BDF1, waves which are smaller than time discretization are completely damped, with SDIRK, which is less dissipative, erroneous oscillations (not necessarily of highest frequency) may be obtained. Then, with too large time steps, SDIRK might produce much less good results than BDF1. This is the reason why we have considered the automatic adaptation of the time step length. Such adaptation is not so easy due to a particular characteristic of the flow: acoustic waves, that are quasi-periodic, and that present amplitudes decreasing progressively of several orders of magnitude. Many classical choices in measuring the time truncation will be faced to the large oscillations of the signal, leading to too large and too small time steps. For example, a sensor relying on the maximum (in domain) of the pressure time derivative:

$$\epsilon_1(t) = \mathrm{Max}_x \partial p/\partial t$$

will produce the "thick" signal presented in Fig. 15.

In our study, we consider

$$\epsilon_i(t) = \partial p/\partial t, \quad \epsilon_{\mathrm{Moy}}(t) = \Sigma_i \epsilon_i(t)/nt,$$

nt being the total number of nodes. Then the actual sensor that we propose is

$$\Delta_{\mathrm{adapt}}(t) = \mathrm{const.} \left(\frac{nt}{\left(\Sigma_i (\epsilon_i(t) - \epsilon_{\mathrm{Moy}}(t))^2 \right)} \right)^{1/2}.$$

The ability of this sensor in evaluating the heterogeneity of the pressure field is much more stable, since, taking the inverse as a time step produces a rather regular time step as illustrated in Fig. 16. In the sequel, and for comparison purpose, we shall also take a logarithmic law (Fig. 16 again) giving a time step evolution close to the adaptative time step.

7.3. Calculation of the whole transient flow

For result evaluation we concentrate on the Nusselt output, a number indicating the rate of calories through

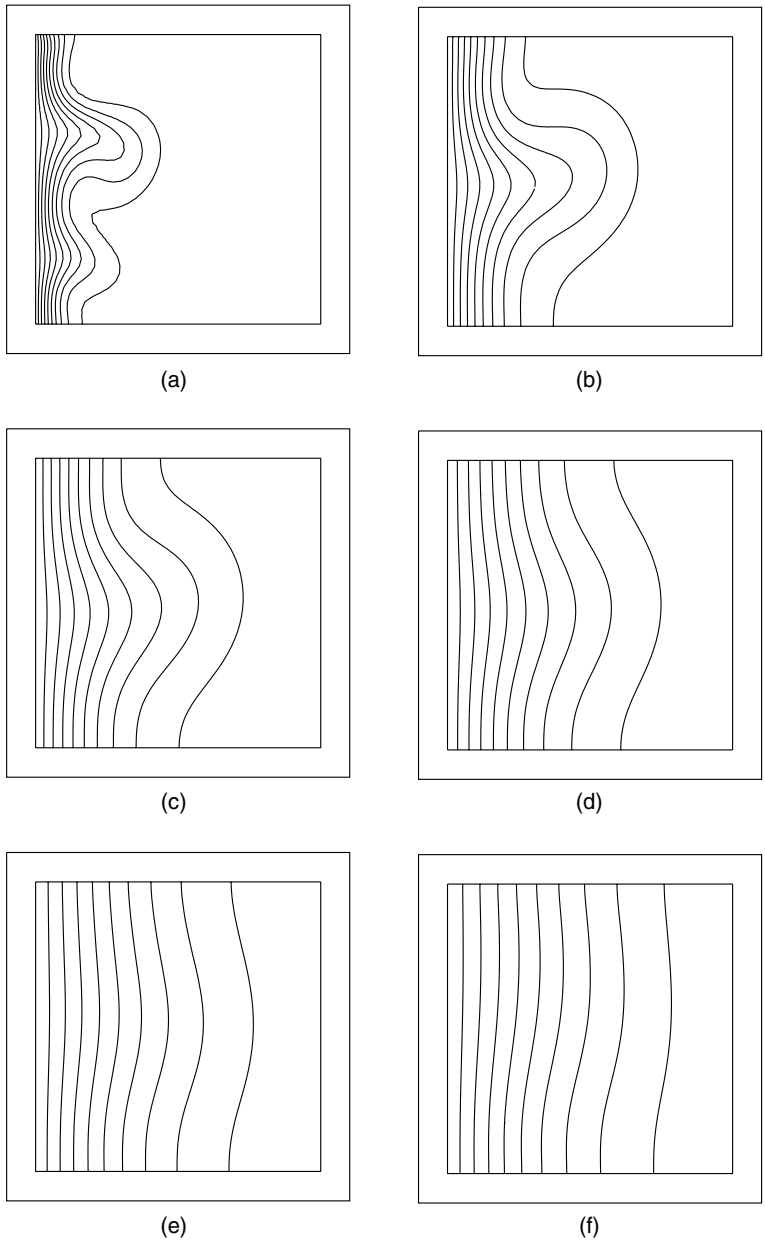

Fig. 14. Unsteady convective flow: temperature contours. (a): $t = 0.1$; (b): $t = 0.5$; (c): $t = 0.9$; (d): $t = 1.3$; (e): $t = 1.7$; (f): $t = 2.1$.

the cold wall. Our time advancing scheme combined with the above time step adaptation is able to produce, for different levels of time discretization, a set of coherent results presented in Fig. 17. We observe time accuracy for smaller time steps at some part of the Nusselt histories and not at some others: the very first interval involves a singular spatial initialization that does not permit third-order accuracy.

Then follows a micro-scale interval, in which the time step is small enough for allowing a high accuracy (third-order in time) and capturing the acoustics transients (t between 0.0001 and 0.001).

Between $t = 0.005$ and $t = 0.05$, the time step increases and progressively reaches the size for which it does not permit anymore the capture of acoustics. Acoustics are then damped by the (yet small) level of dissipation of the time advancing scheme. If we stop the calculation and restart it with a much smaller time step, then acoustic waves reappear instantaneously, see Fig. 18. In the last interval (after $t = 0.05$), our scheme shows

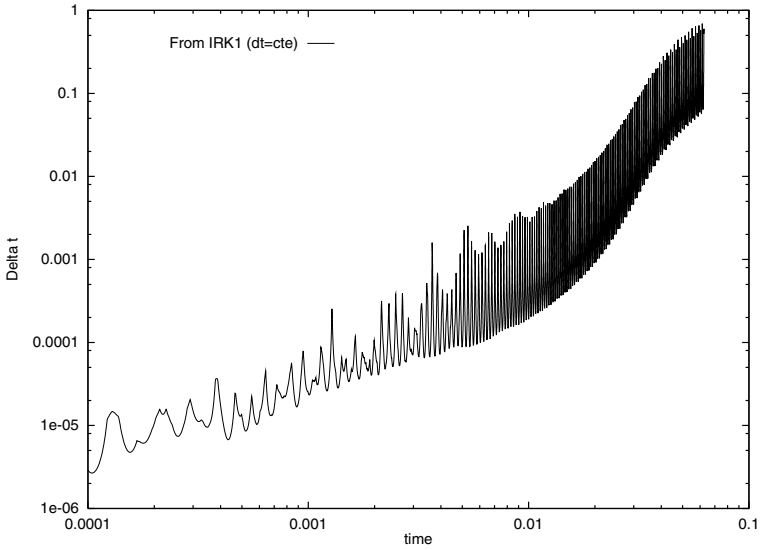

Fig. 15. Transient natural convection; time step adaptation: time step length from the pressure time derivative sensor.

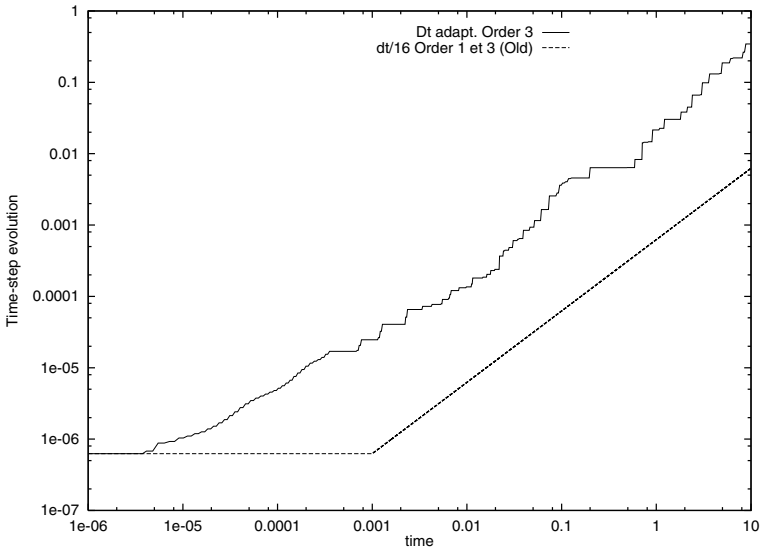

Fig. 16. Transient natural convection: the new adaptive time step length and a simplified time step law close to it.

again an apparent high-order of accuracy, although the time step is too large for convergence at third-order of the truncation error. In fact, errors related to acoustics are of order the square of Mach number and cannot influence much the apparent accuracy of the computation.

To sum up the outputs of this last case study, it appears that the choice of the time step length is a delicate issue. We observe also that, as expected, the third-order accurate implicit scheme is able to capture very fast transients, as far as they are smooth enough, and as far as the time step is small enough. But in that case, the calculation is very expensive.

In cases where acoustic transient are very small, the new scheme can produce accurate answers while dissipating acoustics, as far as large enough time steps are used. Then the scheme can sucessfully compete with schemes of lower order.

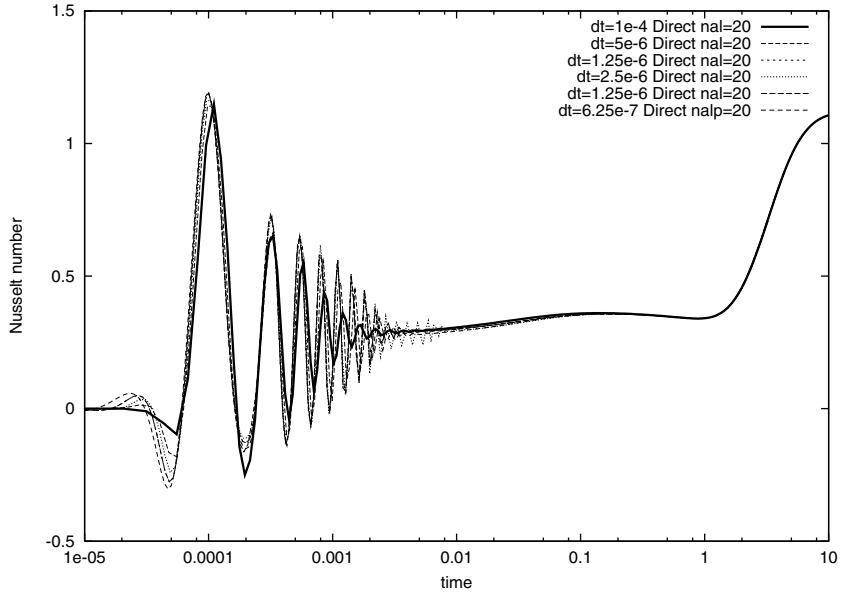

Fig. 17. Transient natural convection: variation of Nusselt number as a function of time (note that the time scale is logarithmic).

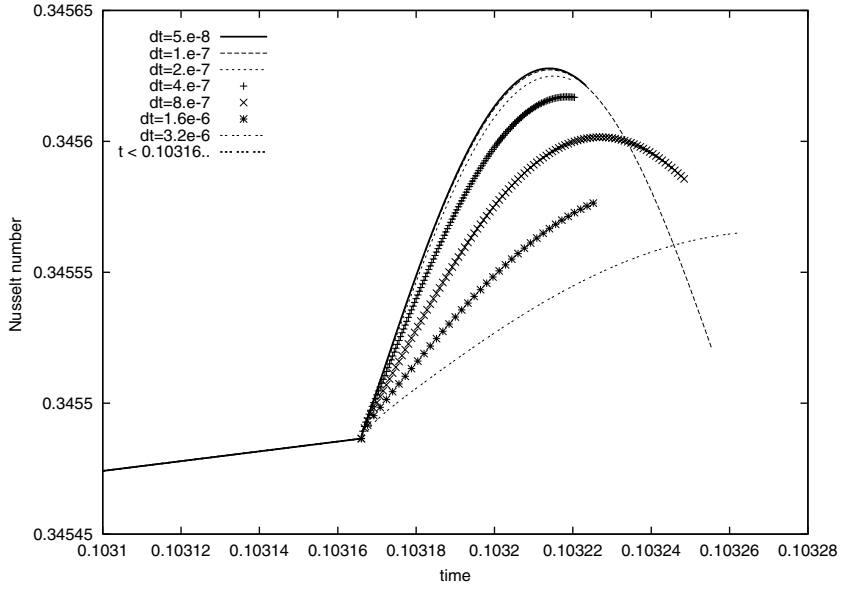

Fig. 18. Transient natural convection: restarting in the acoustics dissipation phase with a much smaller time step provokes the instantaneous rising of acoustics (third-order error convergence is observed for the smallest time step).

8. Concluding remarks

This work contributes to the adaptation of Godunov-type numerical methods to low Mach number flows. Focusing on the Roe flux difference splitting, we analysed the impact of introducing a preconditioner proposed by Turkel in the dissipative term of the Roe splitting. Our first contribution is to show by a truncation analysis that a proper behavior of the truncation error is obtained with this modification not only for incompressible

flow but also for a very large set of asymptotic low Mach number situations, including thermical problems.

Both steady and unsteady problems are targeted and a very popular method for solving them is to use the first-order preconditioning also called defect-correction method. Our second contribution is to propose a simplified analysis for its behavior when applied to low Mach number flows. Iterative convergence is mesh and Mach number independent.

Third, in order to be able to compute accurately unsteady flows, we propose a third-order accurate implicit time advancing enjoying unconditional stability properties. These advances are validated by a set of demonstrative computations.

We showed first that the resulting approximation is able, for an incompressible classical flow case, to provide results with second-order accuracy, and in particular to provide an accuracy as good (for the same number of nodes) as the one obtained by analogous computations performed with the incompressible model and a standard numerical method.

A second case is used for illustrating the performance of the defect-correction iteration. We have described an industrial flow that cannot be computed with asymptotic models (incompressible or dilatable assumptions) but can be well computed with the proposed scheme.

We have proposed an "all time scales" time advancing method of high accuracy, and demonstrated its interest on a complex transient flow involving large and small time scales, with large and small amplitudes.

Further efficiency improvement can be obtained by improving the linear solver for the first-order Jacobian system. Studying it was not in the scope of our study and we refer for example to the fast multi-grid solver developed by Van Leer and co-workers [18].

Also spatial errors can be made smaller by using an upwind stabilisation of even high-order (see for example in [4]).

Concerning the implicit time advancing, some saving may be obtained by replacing the Norsett nonlinear scheme by the linear Rosenbrook one. We have not yet explored this option because we have anyway an inner defect-correction loop which may render the Rosenbrook option not more efficient. The question remains open. Also the issue of computing unsteady flows with fast and slow transients remains a difficult open question that we shall continue to investigate by considering 3D large eddy simulation of low Mach flows.

Acknowledgements

The first author acknowledges the partial support of the University of Pau-Turbomeca convention. Part of this work was done by the second author when she was in post-doctoral position at CEA-Saclay.

References

[1] O. Botella, R. Peyret, Benchmark spectral results on the lid-driven cavity flow, Comput. Fluid. 27 (1998) 421–433.
[2] S. Clerc, Numerical simulation of the homogeneous equilibrium model for two-phase flows, J. Comp. Phys. 161 (2000) 354–375.
[3] G. De Vahl Davis, Natural convection of air in a square cavity: a benchmark numerical solution, Int. J. Numer. Methods Fluids 3 (1983) 227–248.
[4] C. Debiez, A. Dervieux, Mixed element volume MUSCL methods with weak viscosity for steady and unsteady flow calculation, Comput. Fluids 29 (1999) 89–118.
[5] A. Dervieux, J. Periaux, A. Rizzi, B. Van Leer (Eds.), Numerical Simulation of Compressible Euler Flows, Notes in Numerical Fluid Mechanics, vol. 26, Vieweg, 1989.
[6] J.-A. Desideri, P.W. Hemker, Convergence analysis of the defect-correction iteration for hyperbolic problems, SIAM J. Sci. Comput. (1991) 89–118.
[7] L. Fezoui, B. Stoufflet, A class of implicit upwind schemes for Euler simulation with unstructured meshes, J. Comp. Phys. 84 (1989) 174–206.
[8] J. Francescatto, A. Dervieux, A semi-coarsening strategy for unstructured MG based on agglomeration, Int. J. Numer. Methods Fluids 26 (1998) 927–957.
[9] U. Ghia, K.N. Ghia, C.T. Shin, High-*Re* solutions for incompressible flow using the Navier–Stokes equations and a Multigrid method, J. Comp. Phys. 48 (1982) 387–411.
[10] H. Guillard, C. Viozat, On the behavior of upwind schemes in the low Mach number limit, Comput. Fluids 28 (1997) 63–86.
[11] E. Hairer, S.P. Norsett, G. Wanner, Solving Ordinary Differential Equations I, Springer-Verlag, Berlin, 1987.
[12] R. Klein, Semi-implicit extension for a Godunov-type scheme based on low Mach number asymptotics I: one-dimensional flow, J. Comp. Phys. 121 (1995) 213–237.
[13] A. Majda, J. Sethian, The derivation and numerical solution of the equations for zero Mach number combustion, Combust. Sci. Technol. 42 (1985) 185–205.
[14] R. Martin, H. Guillard, A second-order defect-correction scheme for unsteady problems, Comput. Fluids 25 (1996) 9–27.
[15] H. Paillère, C. Viozat, A. Kumbaro, I. Toumi, Comparison of low Mach number models for natural convection problems, Heat Mass Transfer 36 (2000) 567–573.
[16] E. Turkel, Preconditioned methods for solving the incompressible and low speed compressible equations, J. Computat. Phys. 72 (1987) 277–298.
[17] E. Turkel, Review of preconditioning methods of fluid dynamics, Appl. Numer. Math. 12 (1993) 257–284.
[18] E. Turkel, A. Fiterman, B. Van Leer, Preconditioning and the limit to the incompressible flow equations for finite difference schemes, in: M. Hafez, D. Caughey (Eds.), Computing the Future: Advances and Prospects for Computational Aerodynamics, John Wiley and Sons, New York, 1994, pp. 215–234.
[19] B. Van Leer, Towards the ultimate conservative difference scheme, V. A second-order sequence to Godunov's method, J. Computat. Phys. 32 (1979) 101–136.
[20] C. Viozat, Ecoulements stationnaires et instationnaires à petit nombre de Mach et maillages étirés, Ph.D. Thesis, University of Nice, France, 1998.

[21] C. Viozat, Calcul d'écoulement diphasique dans une tuyère: influence de la renormalisation du schéma de flux, Technical Report, CEA, SYSCO/LGLS/RT/00-014, 2000.
[22] P. Wesseling, D.R. van der Heul, C. Vuik, Unified methods for computing compressible and incompressible flows, ECCOMAS 2000, in: Proceedings of the European Congress on Computational Methods in Applied Sciences and Engineering, Barcelona, September, 2000.
[23] P.L. Roe, Approximate Riemann solvers, parameters vectors and difference schemes, J. Comp. Phys. 43 (1981) 357–371.